Title
POTENTIAL ENERGY EFFECTS and DIFFUSION IN THE RELAXED COMPONENTS OF THE REACTION 19'Au + ^Ar AT 288 and 340 MeV BOMBARDING ENERGIES

Author
Moretto, L.G.

Publication Date
1975-09-01

Submitted to Nuclear Physics A

LBL-4084
Preprint c.1

POTENTIAL ENERGY EFFECTS AND DIFFUSION IN THE RELAXED COMPONENTS OF THE REACTION $^{197}Au + ^{40}Ar$ AT 288 AND 340 MeV BOMBARDING ENERGIES

L. G. Moretto, J. Galin, R. Babinet, Z. Fraenkel,
R. Schmitt, R. Jared, and S. G. Thompson

September 1975

Prepared for the U. S. Energy Research and
Development Administration under Contract W-7405-ENG-48

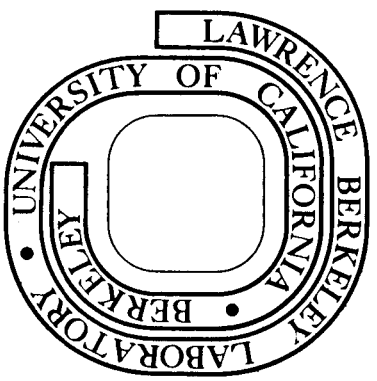

DISCLAIMER

NUCLEAR REACTIONS: $^{40}Ar + ^{197}Au$; $E_{^{40}Ar}$ = 288 MeV, 340 MeV. The emitted fragments have been identified up to Z = 32. Kinetic energy distributions, cross sections and angular distributions have been measured for each Z.

LBL-4084

POTENTIAL ENERGY EFFECTS AND DIFFUSION IN THE RELAXED COMPONENTS OF THE REACTION $^{197}Au + ^{40}Ar$ AT 288 AND 340 MeV BOMBARDING ENERGIES

L. G. Moretto,* J. Galin,† R. Babinet,‡
Z. Fraenkel,§ R. Schmitt, R. Jared and S. G. Thompson

Lawrence Berkeley Laboratory
University of California
Berkeley, California 94720

ABSTRACT

The fragments emitted in the reaction between ^{197}Au and ^{40}Ar at 288 and 340 MeV bombarding energies have been studied. The fragments have been identified in atomic number up to Z = 32 by means of an E-ΔE telescope The kinetic energy distributions, the cross sections and the angular distributions have been measured for each Z. The kinetic energy distributions show the typical quasi elastic and relaxed components; the Z distributions show a smooth increase in the cross section with increasing Z, interrupted at relatively forward angles by a fairly sharp peak close to Z = 18. The angular distributions are forward peaked in excess of $1/\sin\theta$ for atomic numbers as large as $Z \simeq 30$, as far as 12 atomic number units above the projectile; this is at variance with other reactions like Ag + ^{20}Ne, where the angular distributions become $1/\sin\theta$ four or five atomic number units above the projectile. This is interpreted in terms of an enhanced diffusion towards symmetry, possibly promoted by the potential energy in the intermediate complex corresponding to two fragments in contact.

---

*Sloan Fellow 1974 - 1976.

†On leave from Institut de Physique Nucleaire, Orsay, France.

‡On leave from DphN/MF-CEN, Saclay, France.

§On leave from the Weisman Institute, Israel.

I. INTRODUCTION

Recent studies of heavy ion reactions have shown the presence of a component in the cross section characterized by thermalized, or relaxed, kinetic energy distributions.[1-15] The more or less pronounced lack of equilibration, visible in the mass or charge distribution, and especially, the lack of symmetry about 90° in the center of mass angular distributions, rules out a complete association of these reaction products with compound nucleus decay. In the reactions induced by ^{14}N, ^{20}Ne and ^{40}Ar on Ag, a strong dependence of the forward peaking in the angular distribution upon the atomic number of the emitted fragment has been shown.[1-5] The forward peaking in excess of the $1/\sin\theta$ distribution appears to fade away as the Z of the observed fragment is farther removed from the Z of the projectile. Furthermore, an asymmetry in the effect has been observed, namely the fragments with atomic numbers smaller than that of the projectile are more forward peaked than the fragments with atomic number larger than that of the projectile.

The above observations have been interpreted in terms of a diffusion mechanism along the mass asymmetry degree of freedom of an otherwise completely thermalized "intermediate complex" whose shape corresponds approximately to that of two touching fragments.[1-3,5,6] The diffusion along the asymmetry coordinate generates a progressive time delay in the population of fragments with Z's farther removed from that of the projectile. This time delay is reflected in the average decay times of the various fragments. As the average decay time increases and becomes comparable with or greater than the mean rotational period of the "intermediate complex", the angular distributions tend to become symmetric about 90° and to assume the $1/\sin\theta$ shape.

The stronger forward peaking in the angular distribution for fragments with Z's lower than that of the projectile has been interpreted in terms of the potential energy of the intermediate complex along the mass asymmetry coordinate. The entrance channel mass asymmetries of the three above cases (^{14}N, ^{20}Ne and ^{40}Ar on Ag), correspond to a region where the potential energy, expressed in terms of the mass asymmetry degree of freedom, falls rapidly towards extreme asymmetries. Thus the diffusion process drives the system towards large asymmetry resulting in the rapid formation of smaller than the projectile fragments. Heavier fragments can be produced more slowly by "uphill" diffusion.

It appears that a further test of the effect of the potential energy upon the rate of diffusion is desirable, especially if the drift in the diffusion along the mass asymmetry coordinate can be reversed by a suitable choice of the target-projectile system. In the present experiment, this has been tried. The $^{40}Ar + ^{197}Au$ system generated an intermediate complex with an injection asymmetry (asymmetry at the beginning of diffusion) such that the potential energy (as determined from the liquid drop model) decreases substantially *in the direction of symmetry* (see Fig. 5). In this case, diffusion should drive the system towards a fairly rapid formation of fragments larger than the projectile. Thus, a substantial forward peaking in the angular distributions should still appear for fragments much heavier than the projectile.

In a sense this should be an "experimentum crucis" to prove the effect of the potential energy of the intermediate complex upon the time evolution of the system. This kind of evidence, coupled with the relaxed kinetic energy distributions should provide great support to the assumption of a diffusive mechanism responsible for the mass and charge transfer in heavy ion reactions.

II. EXPERIMENTAL TECHNIQUES

The Ar beams at energies corresponding to 7.20 MeV/A (288 MeV) and to 8.5 MeV/A (340 MeV) were provided by the Berkeley SuperHILAC. The beam was collimated to a spot about 3 mm in diameter on the target and was collected by a Faraday cup. Typical intensities of the stripped beam were in the neighborhood of 100 nA electrical. The target thickness ranged between 400 and 600 $\mu g/cm^2$; such a thickness does not appreciably degrade the energies of the beam or of the emitted particles.

Two ΔE,E telescopes mounted on movable arms were used to detect and identify the fragments. The ΔE counters were gas ionization chambers of a type described elsewhere.[2,3,16] The gas used was pure CH_4 at a pressure of approximately 8 cm Hg.

The entrance window of the ΔE counter (Formvar) was approximately 50 $\mu g/cm^2$ thick. The E detector was a Si solid state counter, 300 μm thick. The pulses originating in the two telescopes were fed to standard linear and logic circuitry and were routed to a single ADC system through an analogue multiplexer. The digitized data were fed on line to a PDP-15 computer through a CAMAC system. The data were finally recorded on magnetic tape for off-line analysis. Monitoring of the experiment was performed on line by means of an x,y storage scope and off-line by printing E,ΔE maps. A more detailed presentation of the data acquisition system has been published elsewhere.[2,3]

III. DATA REDUCTION

The data reduction has been performed off-line on a PDP-9 computer. The E,ΔE contour maps generated from the data at each angle show well defined ridges corresponding to the various atomic numbers. The Z resolution is quite good up to and above Z = 32 under optimal conditions. Because

of the great range of energies associated with the various fragments, the optimal resolution has not been attained at all angles. No attempt to analyze the data has been made in the regions where the atomic numbers could not be resolved.

The valleys separating two adjacent elements were identified by means of the coordinates of two or three points in the E-ΔE maps. Then these coordinates were fed to the computer to obtain cross sections and kinetic energy distributions for each Z.

The energy calibration for the E detector was obtained by means of a pulser-chopper system which was checked with the elastically scattered beam. The energy calibration for the ΔE detector was obtained from the energy loss of the elastically scattered beam as computed from the range-energy tables.

Corrections for the mean energy loss inside the target and for the energy loss within the plastic window of the ΔE counter were performed for each atomic number. The corrected differential cross sections $\left.\frac{\partial^2\sigma}{\partial\Omega\partial E}\right|_{lab}$ were transformed to the center-of-mass assuming for each fragment a Z/A ratio equal to that of the combined system. Because of the spread in kinetic energy associated with each Z, a distribution in the center-of-mass angle results. As a consequence, the quoted center of mass kinetic energy distributions correspond to a small distribution of c.m. angles. For each Z the following quantities were calculated in the center of mass:

i) the double differential cross section $\left.\frac{\partial^2\sigma}{\partial\Omega\partial E}\right|_{c.m.}$

ii) the integrated cross section $\left.\frac{d\sigma}{d\Omega}\right|_{c.m.}$

iii) the mean kinetic energy $E_{c.m.} = \left(\frac{d\sigma}{d\Omega}\Big|_{c.m.}\right)^{-1} \int E_{c.m.} \frac{\partial^2\sigma}{\partial\Omega\partial E}\Big| dE_{c.m.}$

iv) the mean angle $\theta_{c.m.} = \left(\frac{d\sigma}{d\Omega}\Big|_{c.m.}\right)^{-1} \int \theta_{c.m.} \frac{\partial^2\sigma}{\partial\Omega\partial E}\Big|_{c.m.} dE_{c.m.}$

More detailed information regarding the data reduction procedure has been published elsewhere.[2,3] Some kinematic features of the reactions are given in Table 1.

IV. THE KINETIC ENERGY DISTRIBUTIONS

In this reaction, as in other previously studied heavy ion reactions, the kinetic energy spectra are characterized by two components: a high energy component which we call "quasi elastic", and a low energy component which we call "relaxed". The relaxed component is common to all fragments and to all angles, while the quasi elastic component is restricted to particles with Z close to that of the projectile and to angles close to the grazing angle. The decomposition is not always so obvious for particles of $Z < 18$ where broad kinetic energy distributions, whose widths depend strongly upon angle, are observed. Examples of center-of-mass kinetic energy distributions are shown in Fig. (1). It can be seen that, at least at backward angles, the relaxed kinetic energy distributions are quite constant and independent of angle. The most probable kinetic energies for each Z as a function of center-of-mass angle are shown in Fig. 2. One can observe that, at sufficiently backward angles, the average kinetic energies become independent of angle. At the forward angles close to the grazing angle, the mean kinetic energies tend to become larger. This is particularly true close to $Z = 18$, but it is also quite evident for other particles with $Z < 18$.

In Fig. 2 the widths (FWHM) are also shown for various Z's. Again, the widths tend to become constant with increasing angle. A constant width is attained at relatively small angles for $Z > 18$, at somewhat larger angles for $Z < 18$. The last figure gives a good idea of the angular range over which the relaxed component of the cross section is essentially free from quasi elastic contributions.

A plot of the mean center-of-mass kinetic energies as a function of Z (Fig. 3) shows that these energies are strongly correlated with the energies expected to arise from Coulomb repulsion. The energies obtained from the Coulomb repulsion of two touching spheres, and those obtained from the Coulomb repulsion of two touching spheroids allowed to attain their equilibrium deformation, are also shown in the figure for comparison. While some doubts may remain as to which configuration is responsible for the final kinetic energy, the association of the experimentally observed kinetic energies with those of the calculated to arise from Coulomb repulsion is unmistakable. These features are in complete agreement with the results obtained from other heavy ion reactions.

The conclusions that can be drawn from the study of the kinetic energy distributions are uncertain. The only relatively clear conclusion refers to the relaxed component. Its fission-like appearance suggests a nearly complete statistical equilibration of the kinetic energies with the internal degrees of freedom.[17] One can presumably expect a good deal of ordinary fission to be involved in these reactions, and its mass/charge distribution could well extend down below $Z = 30$. And yet lack of symmetry about 90° in the angular distributions, which we shall consider later, indicates the presence of a faster process. Such a process we have associated with the formation of an intermediate complex, retaining the approximate shape of two touching fragments, and diffusing along the mass asymmetry degree of freedom.[1-3,6,7] It is not clear at the moment how to

separate two such components, namely the fission and the diffusion components.

The quasi elastic component at times appears as a well defined peak; at others it appears to mix with the relaxed component, thus generating broad distributions. In fact in these cases it is not at all clear whether it is legitimate to assume the existence of two distinct processes or whether one is dealing with a continuum of intermediate stages of relaxation.

V. THE CHARGE DISTRIBUTION

The laboratory cross sections at each angle are plotted as a function of atomic number in Fig. 4 for both energies. The center of mass cross sections integrated over a fixed angular range are given in Table 2. The general appearance of these cross sections is quite similar at both bombarding energies. At forward angles a very sharp peak is visible close to $Z = 18$. This peak is quite asymmetric. To the right, for $Z > 18$, the cross section drops very rapidly, while to the left, for $Z < 18$, it decreases rather slowly. For sufficiently large laboratory angles, for instance $\theta_{lab} = 70°$ at 288 MeV bombarding energy and $\theta_{lab} = 60°$ at 340 MeV bombarding energy, the peak is absent and the cross sections appear to vary smoothly with Z. The asymmetry of the peak is closely associated with the kinetic energy spectra. Above $Z = 18$, the kinetic energy spectra are relaxed and their width is essentially constant throughout the entire angular range. Below $Z = 18$, the kinetic energy spectra cannot be easily separated into the relaxed and quasi elastic components. The cross sections reported here are obtained by integrating the kinetic energy spectrum irrespective of its width. Therefore they may incorporate a substantial amount of quasi elastic cross section which, not surprisingly, is concentrated about the atomic number of the projectile.

Still, the physical reason for the asymmetry is not clear, in other words, it is not understood why the quasi elastic component is prevailing for $Z < 18$. The observation that this excess cross section may be due to the break-up of the projectile could be of significance, but at this stage, this is just an observation and not an explanation.

The distributions observed at large angles, and thus associated with the relaxed component of the kinetic energy spectrum are, in a sense, now quite familiar. There is a somewhat larger cross section for the very light Z's, rapidly decreasing to a minimum around $Z = 9$, followed by a dramatic increase in cross section with increasing Z, covering a range of almost two orders of magnitude from $Z = 9$ to $Z = 28$-29. These features qualitatively resemble those observed in the reaction Ag + Ar,[2,4,5] though in that reaction the rise in cross section with Z is not quite as dramatic. Again, the correlation between the general trend of these cross sections with Z and the potential of the intermediate complex as a function of Z (Fig. 5) is quite compelling and easily observable in Fig.(6). The potential shows the Businaro Gallone mountains well displaced toward small Z's and the potential sloping quite dramatically on both sides towards both small and large Z's. Thus, if one expects that the yield be approximately proportional to the Boltzmann factors:

$$Y(Z) = k(Z,T) \exp(-V_Z/T)$$

one obtains a good qualitative explanation of the observed distributions. On the other hand, as observed elsewhere, the qualitative agreement between the experiment and this statistical prediction only indicates that the mechanism responsible for the observed cross section is sensitive to the ratio V_Z/T. It does not imply automatically that the distribution is

purely statistical in nature. Further evidence of a V_Z/T effect can be seen in the cross sections when plotted as a function of angle for each Z (Fig. 7). At small Z's the cross sections for the 288 MeV bombarding energy are lower than the corresponding cross sections for the 340 MeV bombarding energy. At large Z's the opposite is true, namely the cross section for 288 MeV is actually *larger* than that for 340 MeV. The pivoting Z appears to be somewhere between 18 and 21. This can be explained as a V_Z/T effect, whereby, at the larger energy (or temperature), the regions of high and low potential are more nearly equalized in the cross section than at the lower energy (or temperature). In this respect, it is quite possible that the unknown change in ℓ window associated with the change in bombarding energy may be partially responsible for such an effect. However, the explanation in terms of temperature change seems more plausible.

As a general comment, the similarity of the Z distribution of the relaxed component with fission is quite striking. One can hardly avoid the association of the observed distribution with the left-hand side tail of a fission distribution. And yet, at least up to Z = 30, asymmetric angular distributions indicate that there is at least part of the cross section which cannot be called just fission. And even for the rest of the cross section, higher up in Z, one must be dealing with a very peculiar kind of fission, with a compound nucleus that has hundreds of MeV of excitation energy and, even at the lowest ℓ wave has hardly any fission barrier left.

VI. THE ANGULAR DISTRIBUTIONS

The center-of-mass angular distributions for the fragments of various atomic numbers and for both 288 MeV and 340 MeV bombarding energies

are shown in Fig. (7). In these graphs, any quasi elastic component of the cross section identified as a separate peak has been eliminated. For the case in which no decomposition of the kinetic energy spectrum appeared to be feasible, the point has not been plotted. This procedure has been adopted in the attempt to obtain angular distributions for the relaxed components only. Unfortunately, as noted before, for atomic numbers below $Z = 18$ the kinetic energy spectra in the forward direction appear to be anomalously broad. In other words, for these fragments either the relaxation of the kinetic energy is not complete or the quasi elastic component severely overlaps with the relaxed component, so that no correct decomposition is possible. Consequently, it is not clear how to interpret these angular distributions, because the kinetic energy spectra change quite substantially in width when one moves from forward to backward directions. The very strong forward peaking of these angular distributions appears to be associated more with the presence of a non-relaxed component than otherwise. It is quite possible that for higher bombarding energies, the overlapping of quasi elastic and relaxed components is not so severe.

On the other hand, the fragments with $Z > 18$ do not suffer from such a problem. The kinetic energy spectra become relaxed at reasonably forward angles and their widths remain constant for more backward angles. Consequently it appears possible to study the angular distributions of the relaxed component of the kinetic energy for fragments with $Z > 18$. Inspection of these angular distributions shows that the excess forward peaking is retained for fragments with Z well above 18. At the lower bombarding energy, the angular distributions are more sharply forward peaked than at the higher bombarding energy and the minimum is more displaced towards the

backward hemisphere. In both cases the excess forward peaking slowly decreases with increasing Z. However, the limiting $1/\sin\theta$ form of the angular distribution seems to be attained only around Z = 29-30. This is to be contrasted with the results obtained for different systems, like N + Ag, Ne + Ag, or Ar + Ag,[1-6] where the $1/\sin\theta$ limit is attained only four to five Z units above the projectile. In the present case, the system must diffuse more than ten Z units above the projectile before the $1/\sin\theta$ limit is attained. This evidence appears to be in good support of the diffusion hypothesis. As was mentioned in the Introduction, the injection points for N + Ag and Ne + Ag are located to the left or close to the top of the Businaro-Gallone mountain in the potential energy vs. asymmetry curve of the intermediate complex, a region where the potential energy slopes down rapidly towards the extreme mass asymmetries. In the case of Ag + Ar the injection point is somewhat to the right of the Businaro-Gallone summit. However, the potential energy trough at symmetry is not well developed for most of the ℓ waves, so that, for Z > 18, the potential energy is rather flat. In the present case of Au + Ar, the injection point is well to the right of the Businaro-Gallone mountain, in a region where the potential energy is steeply falling towards symmetry. Consequently, in the latter case, diffusion is driven by the potential energy towards large Z's, which in turn, permits their early decay and results in forward peaking. In the former cases the potential energy either hampers or does not help diffusion to populate large Z's, thus resulting in a rapidly fading forward peaking.

A possible temperature effect is also seen in the angular distributions at the two energies. At the lower energy the angular distributions appear to be sharper than at the higher energy, perhaps because the

diffusion process depends upon V_Z/T and not upon V_Z alone. Thus the higher temperature appears to reduce the drift velocity associated with the potential energy.

VII. CONCLUSION

In the reaction studied in the present work, the very same patterns visible in previously studied systems have been observed. The kinetic energies present both the "quasi elastic" and the "relaxed" components and the latter is similar to what is to be expected from fission. The Z distribution, once the quasi elastic component is excluded, is very smooth and seems to reflect the qualitative pattern to be expected from the potential energy studies. The angular distributions of the relaxed component are forward peaked and, differently from previously discussed systems, retain their forward peaking up to very large Z (Z = 29-30) or 11 atomic numbers above that of the projectile. This has been interpreted in terms of the diffusion model proposed by Moretto and Sventek.[7] The potential energy of the intermediate complex, which is rapidly decreasing towards symmetry, generates a rapid drift towards large atomic numbers thus keeping the time delay between injection and decay fairly short for each atomic number. In turn this seems to reflect itself on the forward peaking of the angular distributions.

A serious argument, still open, is whether this decay process associated with diffusion is mixed with ordinary fission, and if so, how to separate the two. Unfortunately in this range of angular momenta and excitation energies, the ordinary compound nucleus theories are expected to be unreliable, because of vanishingly small fission barriers and

because of predicted decay times of the order of, or shorter than, the predicted collective periods of the compound nucleus.

REFERENCES

1. L. G. Moretto, S. K. Kataria, R. C. Jared, R. Schmitt and S. G. Thompson, Lawrence Berkeley Report LBL-4063, May 1975.

2. J. Galin, L. G. Moretto, R. Babinet, R. Schmitt, R. Jared and S. G. Thompson, Lawrence Berkeley Report LBL-4064, June 1975.

3. R. Babinet, L. G. Moretto, J. Galin, R. Jared, J. Moulton and S. G. Thompson, Lawrence Berkeley Report LBL-4080, July 1975.

4. L. G. Moretto, D. Heunemann, R. C. Jared, R. C. Gatti and S. G. Thompson, Physics and Chemistry of Fission 1973, International Atomic Energy Agency, Vienna, 1974 V. II, p. 351.

5. S. G. Thompson, L. G. Moretto, R. C. Jared, R. P. Babinet, J. Galin, M. M. Fowler, R. C. Gatti and J. B. Hunter, Nobel Symposium on Superheavy Elements (1974). Physica Scripta Vol. 10-A.

6. L. G. Moretto, R. P. Babinet, J. Galin and S. G. Thompson, Lawrence Berkeley Report LBL-3444, November 1974, to be published in Physics Letters.

7. L. G. Moretto and J. S. Sventek, Lawrence Berkeley Report LBL-3443, November 1974, to be published in Physics Letters.

8. J. Galin, D. Guerreau, M. Lefort, J. Péter and X. Tarrago, Nucl. Phys. A 159 (1970) 461.

9. A. G. Artukh, V. V. Avdeichikov, G. F. Gridnev, V. L. Mikheev, V. V. Volkov and J. Wilczinski, Nucl. Phys. A 167 (1971) 284.

10. A. G. Artukh, G. F. Gridnev, V. L. Mikheev, V. V. Volkov and J. Wilczinski, Nucl. Phys. A 211 (1973) 299.

11. A. G. Artukh, G. F. Gridnev, V. L. Mikheev, V. V. Volkov and J. Wilczinski, Nucl. Phys. A 215 (1973) 91.

12. F. Hanappe, C. Ngô, J. Péter, B. Tamain, Physics and Chemistry of Fission 1973, International Atomic Energy Agency, Vienna, 1974 V. II, p. 289.

13. F. Hanappe, M. Lefort, C. Ngô, J. Péter and B. Tamain, Phys. Rev. Lett. 32 (1974) 738.

14. K. L. Wolf, J. P. Unik, J. R. Huizenga, V. E. Viola, J. Birkelund and H. Freiseleben, Phys. Rev. Lett. 33 (1974) 1105.

15. For a complete list of references see A. Fleury and J. M. Alexander, Ann. Rev. Nucl. Sci. 1632-4 (1974) 279.

16. M. M. Fowler and R. C. Jared, Nucl. Instr. Meth. 124 (1975) 341.

17. L. G. Moretto, Lawrence Berkeley Report LBL-3454, January 1975, to be published in Nucl. Phys.

FIGURE CAPTIONS

Fig. 1. Examples of center-of-mass kinetic energy distributions for various atomic numbers. The quasi elastic components are seen as separate peaks for atomic numbers close to that of the projectile. For $Z > 18$ the quasi elastic peak is small and well separated, while for $Z < 18$ the quasi elastic and the relaxed peaks merge into each other. At large angles the relaxed peaks become the only components of the distributions.

Fig. 2. Most probable kinetic energies and widths (FWHM) in the center-of-mass as a function of the center-of-mass angle. The widths are displayed as error bars. The most probable energies and widths are largest at angles somewhat smaller than the grazing angle. This is particularly visible at 288 MeV bombarding energy.

Fig. 3. Average values for the most probable kinetic energies and for the widths (FWHM) of the kinetic energy distributions. The averages have been performed over the angular ranges where only the relaxed component is dominant, namely between 70° and 157° (lab) at 288 MeV and between 50° and 157° (lab) at 340 MeV bombarding energies. The two curves correspond to the kinetic energies expected from Coulomb repulsion of two touching spheres and of two touching spheroids at equilibrium deformation.

Fig. 4. Laboratory differential cross sections $\left.\frac{d\sigma}{d\Omega}\right|_{lab}$ as a function of atomic number for various laboratory angles. Filled points indicate that the cross section was obtained by integrating a relaxed kinetic energy distribution. Open symbols indicate either the presence of a quasi elastic component or that the kinetic energy distribution was unusually broad. Notice how the peak around $Z = 18$ disappears at backward angles.

Fig. 5. Potential energy of the intermediate complex relative to the corresponding HISKES shape as a function of the atomic number of one of the fragments for various ℓ values. The calculation has been performed for a configuration of two spherical liquid drops in contact.

Fig. 6. Center-of-mass differential cross section $\left.\frac{d\sigma}{d\Omega}\right|_{c.m.}$ as a function of atomic number interpolated at various center-of mass angles.

Fig. 7. Center-of-mass angular distributions for various atomic numbers. The quasi elastic contributions have been subtracted when present as a distinct peak. This could not be done for $Z < 18$. The dashed curves plotted for $Z = 27$, 28 and 29 correspond to $1/\sin\theta$ distributions.

TABLE I

Characteristics of the reaction $^{197}_{79}Au + ^{40}_{18}$ at two bombarding energies.

	^{40}Ar Lab Energy (MeV)	
	288	340
$E_{c.m.}$ (MeV)	239.	283.
$E^*_{c.n.}$	226.	269.
$T_{c.n.}$ (MeV)	2.8	3.0
L_{max} ((ħ)	156.	191.
σ_r (b)	1.99	2.54
$\theta_{grazing,\ lab}$ (deg)	48°.	37°.
$B_{Coulomb}$ (MeV)	154.	154.

An r_o of 1.225fm was used to calculate nuclear radii. In addition, 2.0 fm were added to the sum of the nuclear radii in the calculation of the reaction cross section σ_r, Coulomb barrier $B_{Coulomb}$, maximum angular momentum L_{max}, and grazing angle $\theta_{grazing}$. The temperatures $T_{c.n.}$ were calculated from $T_{c.n.} = \sqrt{E^*_{c.n.}/a}$ assuming a = A/8 and ℓ = 0 ħ.

TABLE 2: Integrated center of mass cross sections for the observed charges. The limits of integration θ_1 and θ_2 define the angular range of experimental data where the relaxed component dominated. The cross sections for this range are given in the next column. The last column gives cross sections obtained from polynomial fits to the data from 30° to 130°. Because of the experimental errors and errors introduced in the interpolation and extrapolation procedure, the quoted values may be in error by as much as 20%.

Z	θ_1	θ_2	$2\pi\int_{\theta_1}^{\theta_2} \frac{d\sigma}{d\Omega} \sin\theta d\theta$	$2\pi\int_{30°}^{130°} \frac{d\sigma}{d\Omega} \sin\theta d\theta$	θ_1	θ_2	$2\pi\int_{\theta_1}^{\theta_2} \frac{d\sigma}{d\Omega} \sin\theta d\theta$	$2\pi\int_{30°}^{130°} \frac{d\sigma}{d\Omega} \sin\theta d\theta$
	deg	deg	mb	mb	deg	deg	mb	mb
	E= 288 MeV				E = 340 MeV			
10	25	105	1.56	1.59	32	77	2.02	10.42
11	24	141	3.53	2.67	32	117	3.64	3.94
12	86	163	0.57	3.31	32	163	5.87	6.07
13	85	163	0.62	4.01	39	163	5.25	7.29
14	85	163	0.73	7.12	62	163	2.18	4.62
15	85	163	0.84	3.98	62	163	2.42	4.81
16	85	163	1.10	3.15	62	163	2.87	5.99
17	84	163	1.22	5.08	62	163	3.67	7.35
19	85	163	2.25	6.18	63	164	5.09	8.81
20	85	163	2.71	7.48	50	164	8.10	11.38
21	85	163	3.80	5.11	51	151	7.95	11.06
22	85	164	4.73	11.25	51	152	9.12	11.86
23	86	164	5.56	12.60	52	144	9.56	13.23
24	86	164	6.49	13.21	52	137	9.73	14.14
25	26	158	20.06	16.53	52	119	8.64	13.54
26	26	143	21.52	18.99	52	120	9.18	14.07
27	26	143	22.34	19.66				
28	26	136	23.89	21.85				
29	26	119	21.67	22.92				
30	26	88	17.26	22.81				

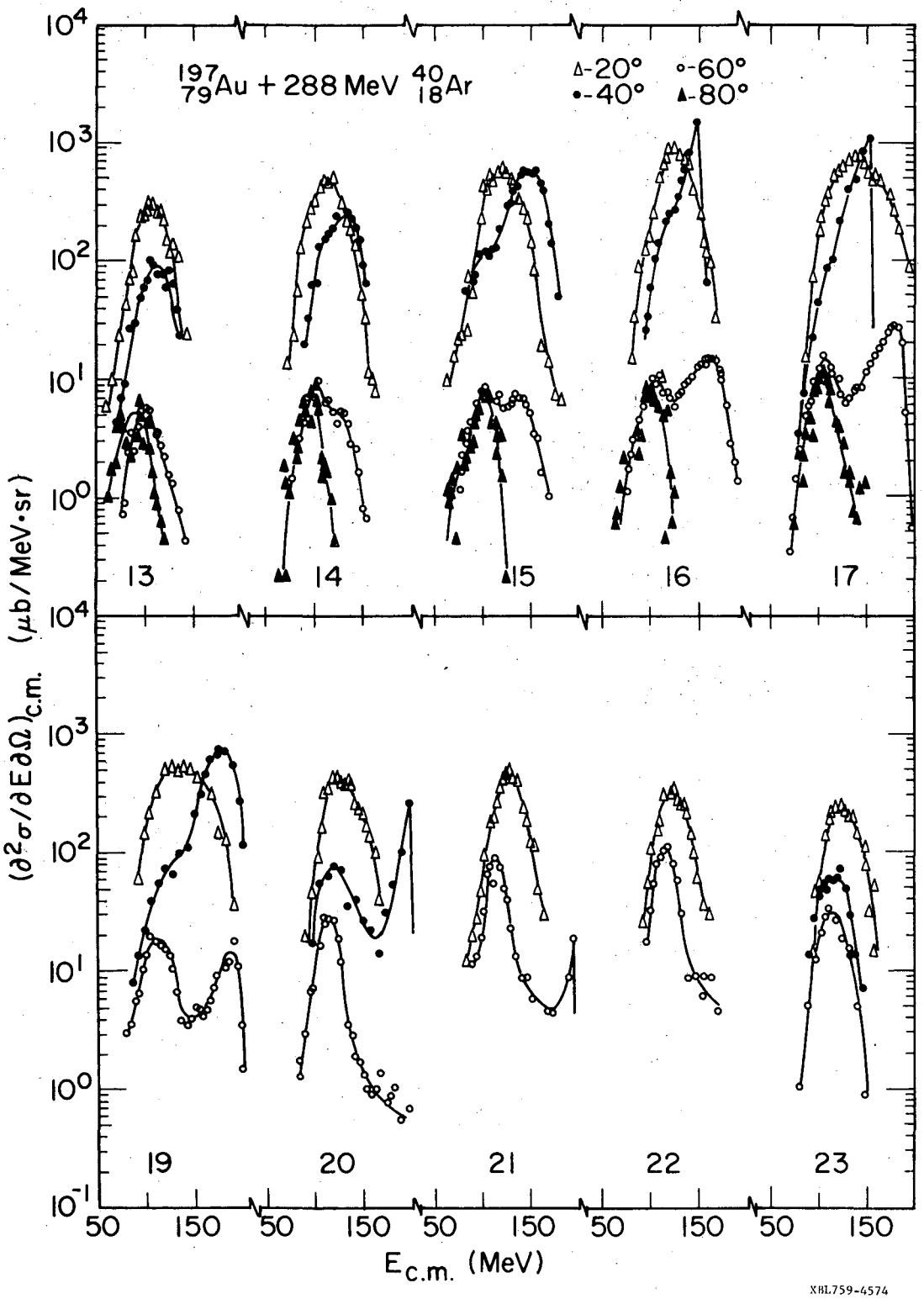
197 79 Au + 288 MeV 40 18 Ar
Δ-20°
∘-60°
•-40°
▲-80°
13
14
15
16
17
19
20
21
22
23
(∂²σ/∂E∂Ω)c.m. (μb/MeV·sr)
Ec.m. (MeV)
XBL759-4574

Fig. 1a

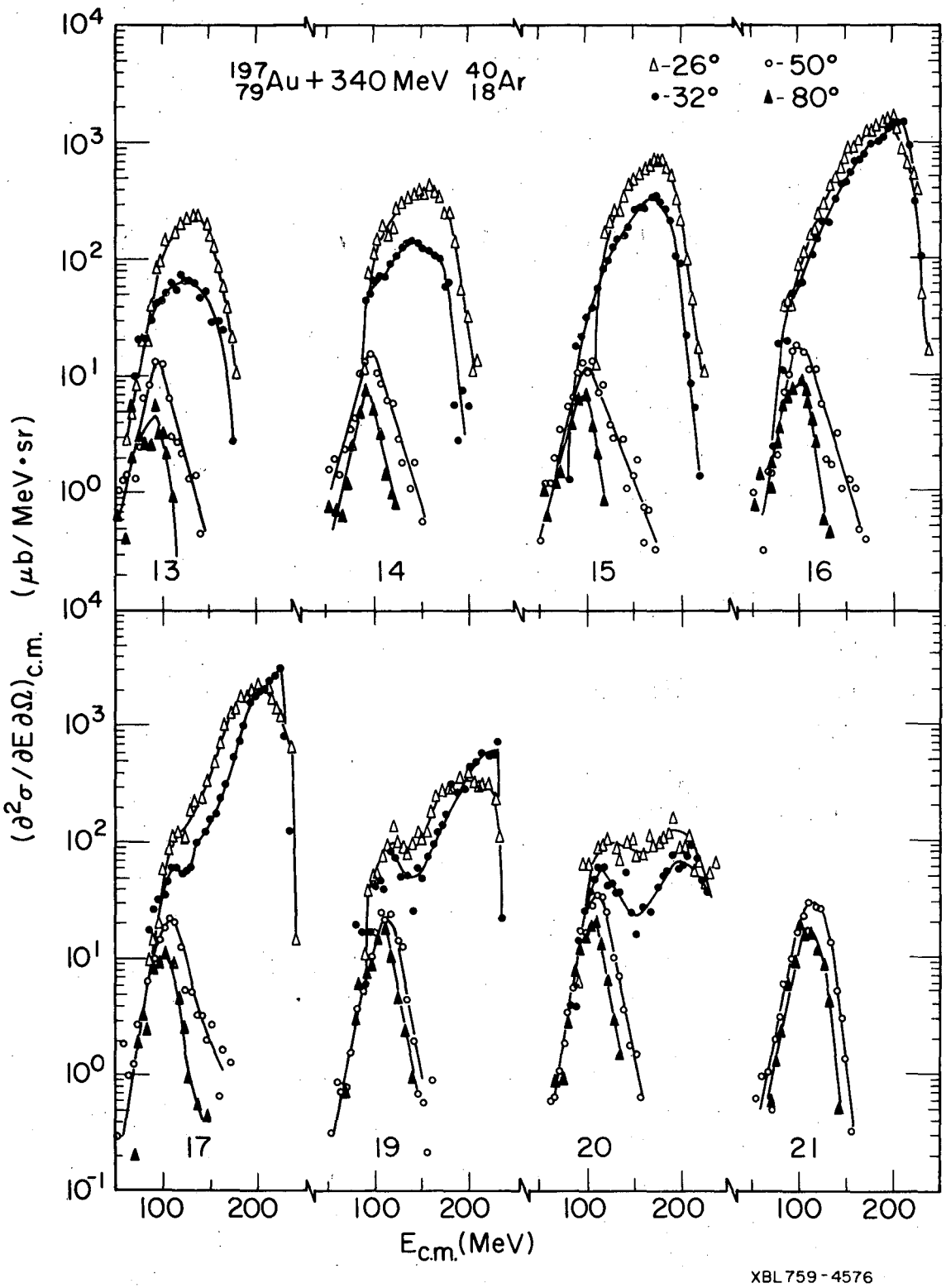

Fig. 1b

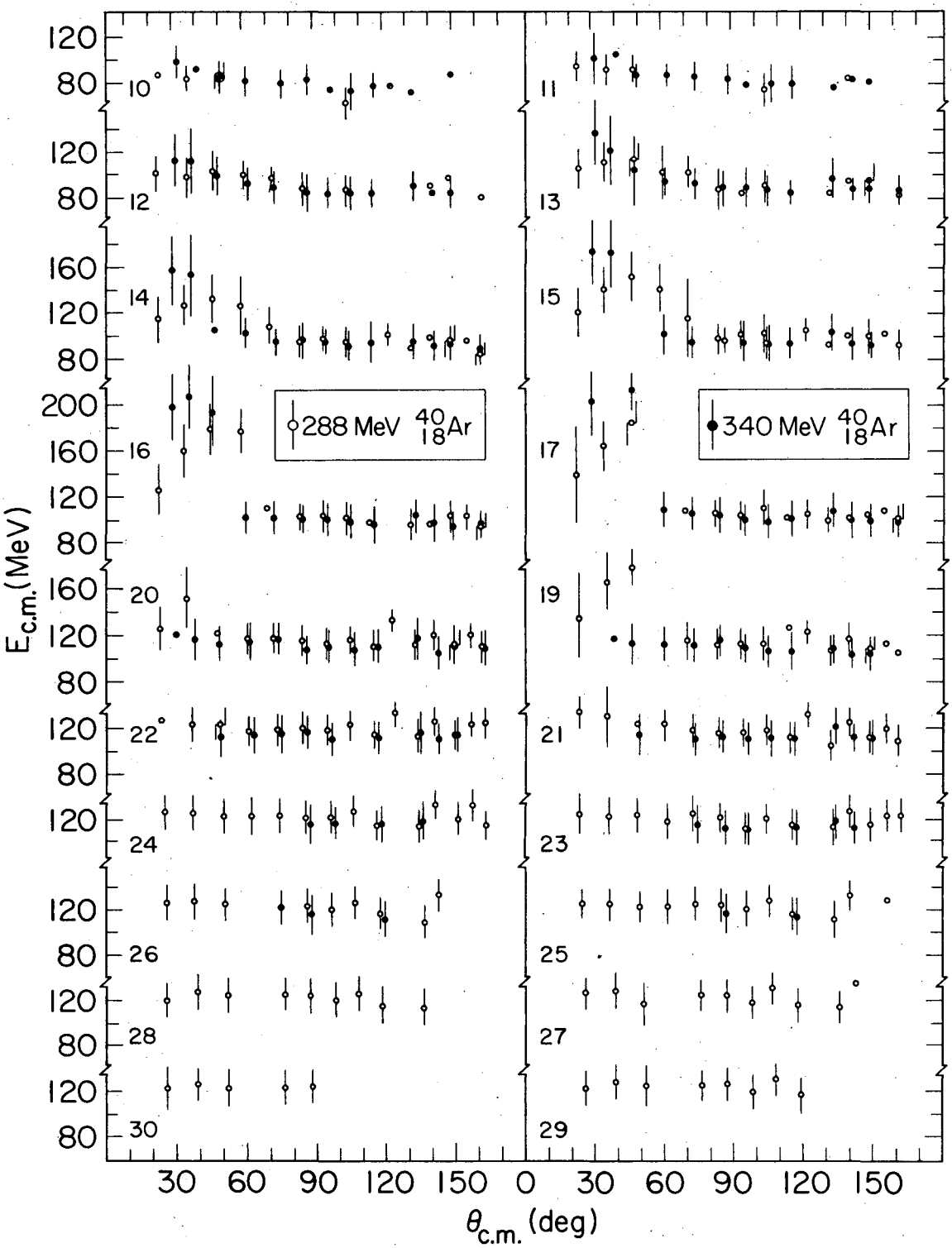

Fig. 2

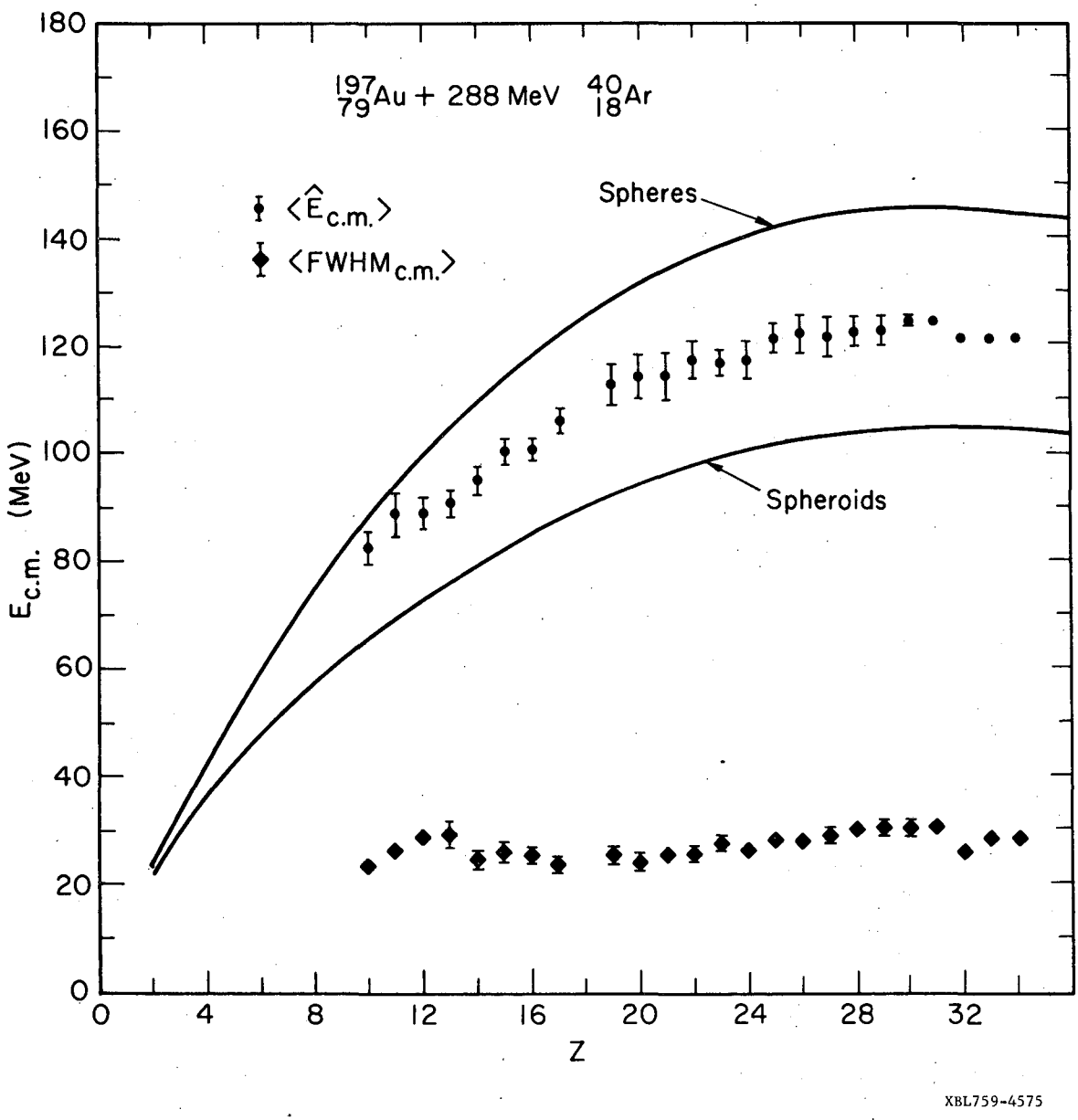

Fig. 3a

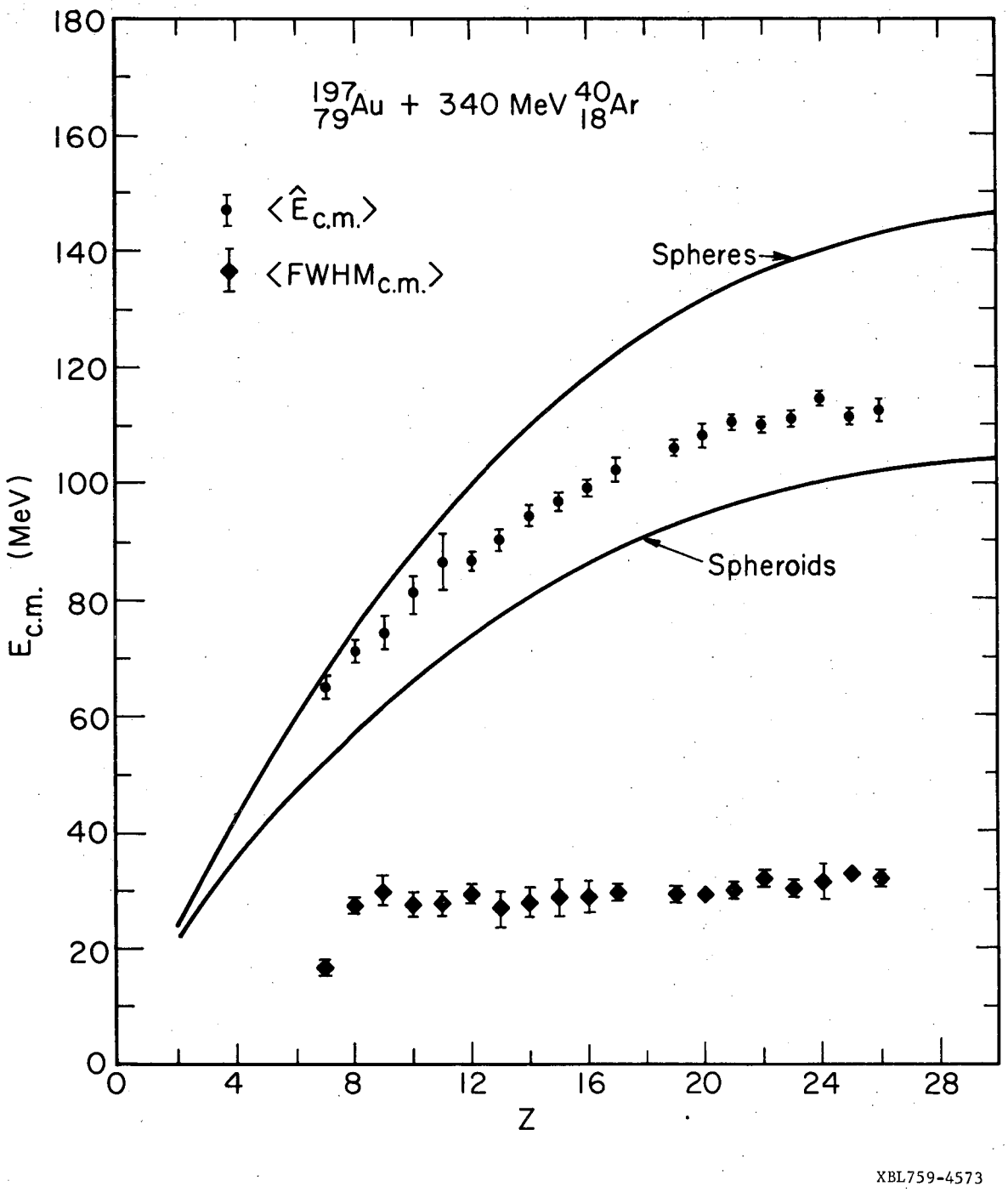

XBL759-4573

Fig. 3b

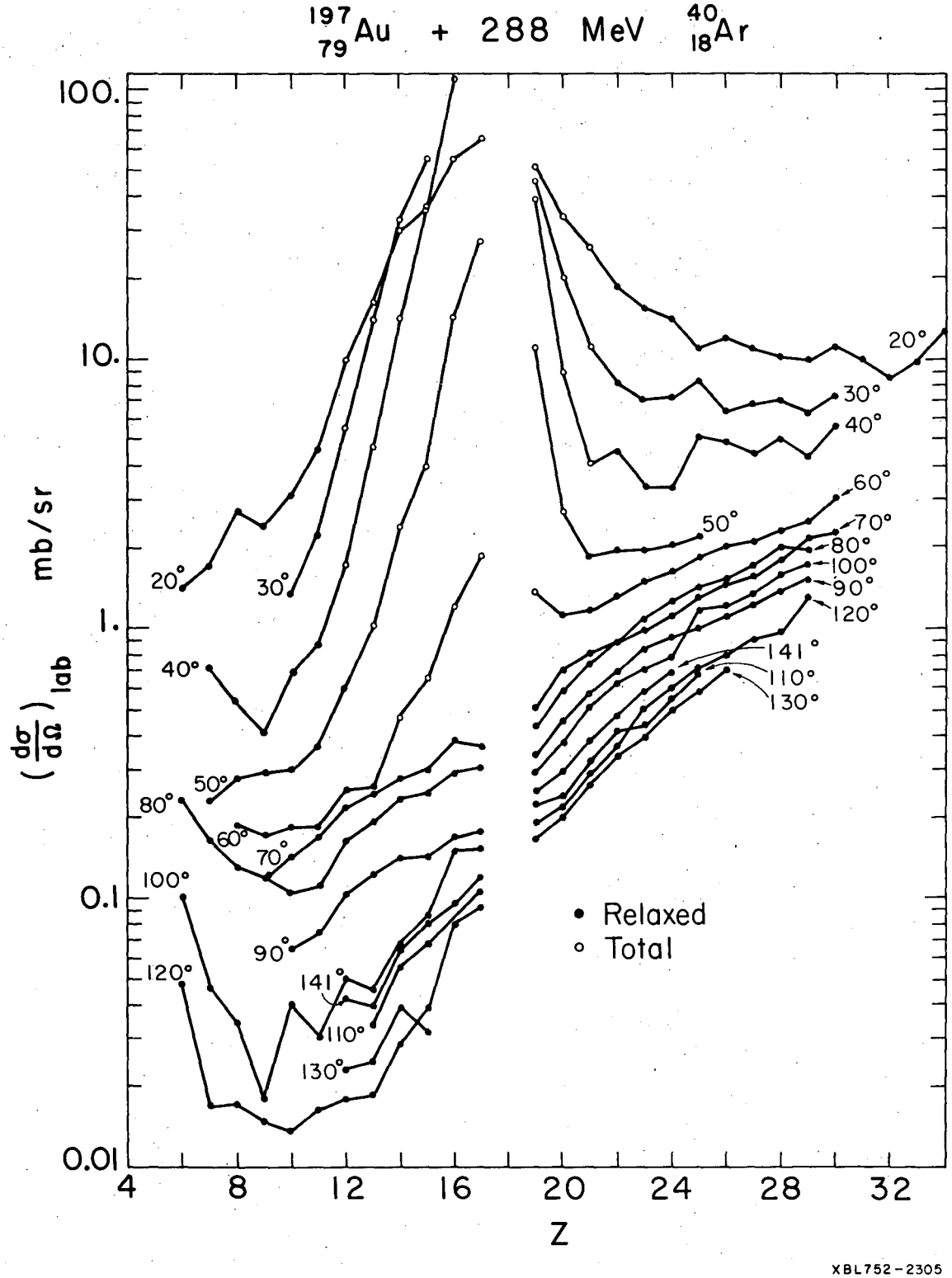

Fig. 4a

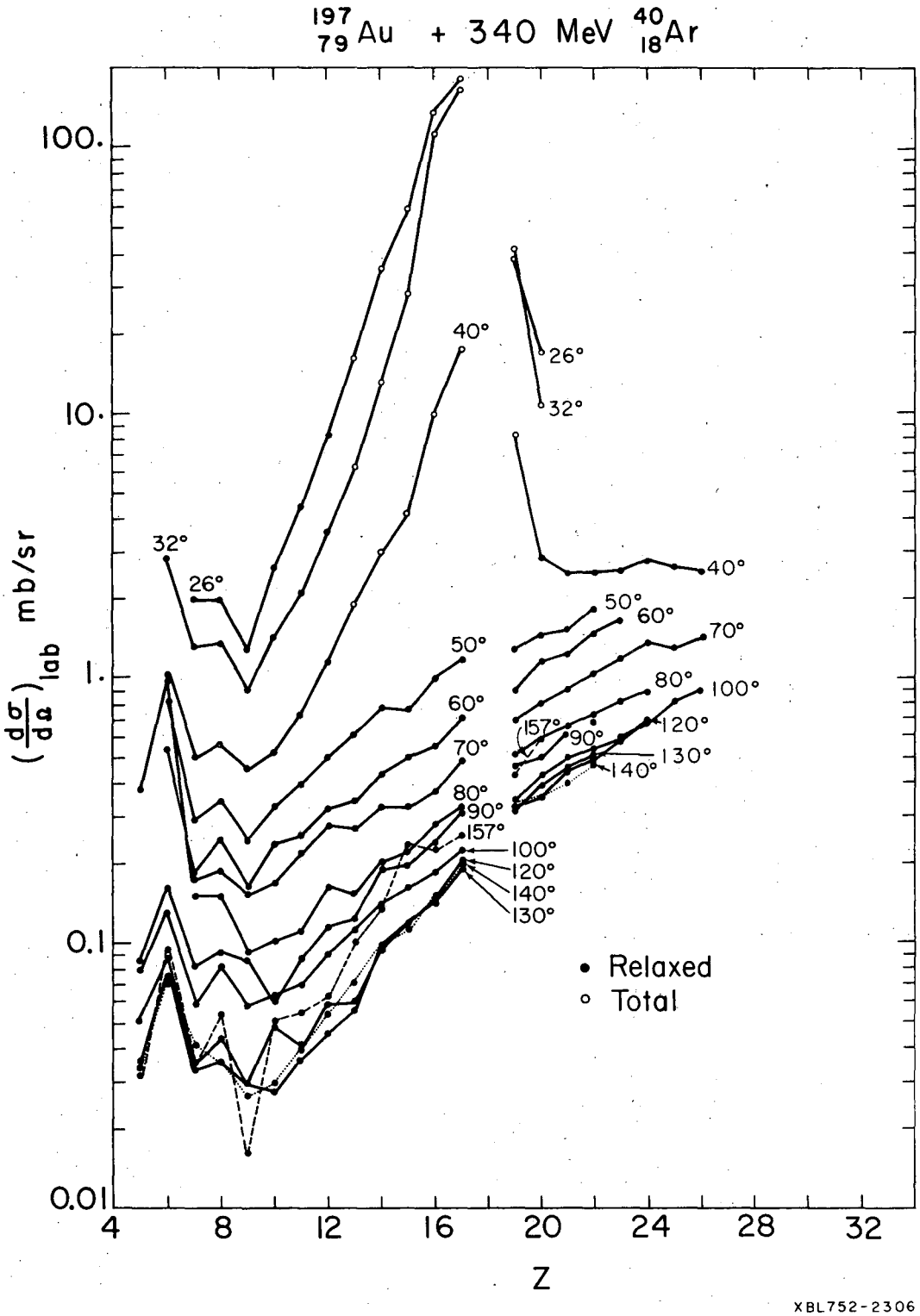
197 79 Au + 340 MeV 40 18 Ar
100.
10.
1.
0.1
0.01
(dσ/dΩ)lab mb/sr
4
8
12
16
20
24
28
32
Z
32°
26°
40°
50°
60°
70°
80°
90°
157°
100°
120°
140°
130°
• Relaxed
○ Total
XBL752-2306

Fig. 4b

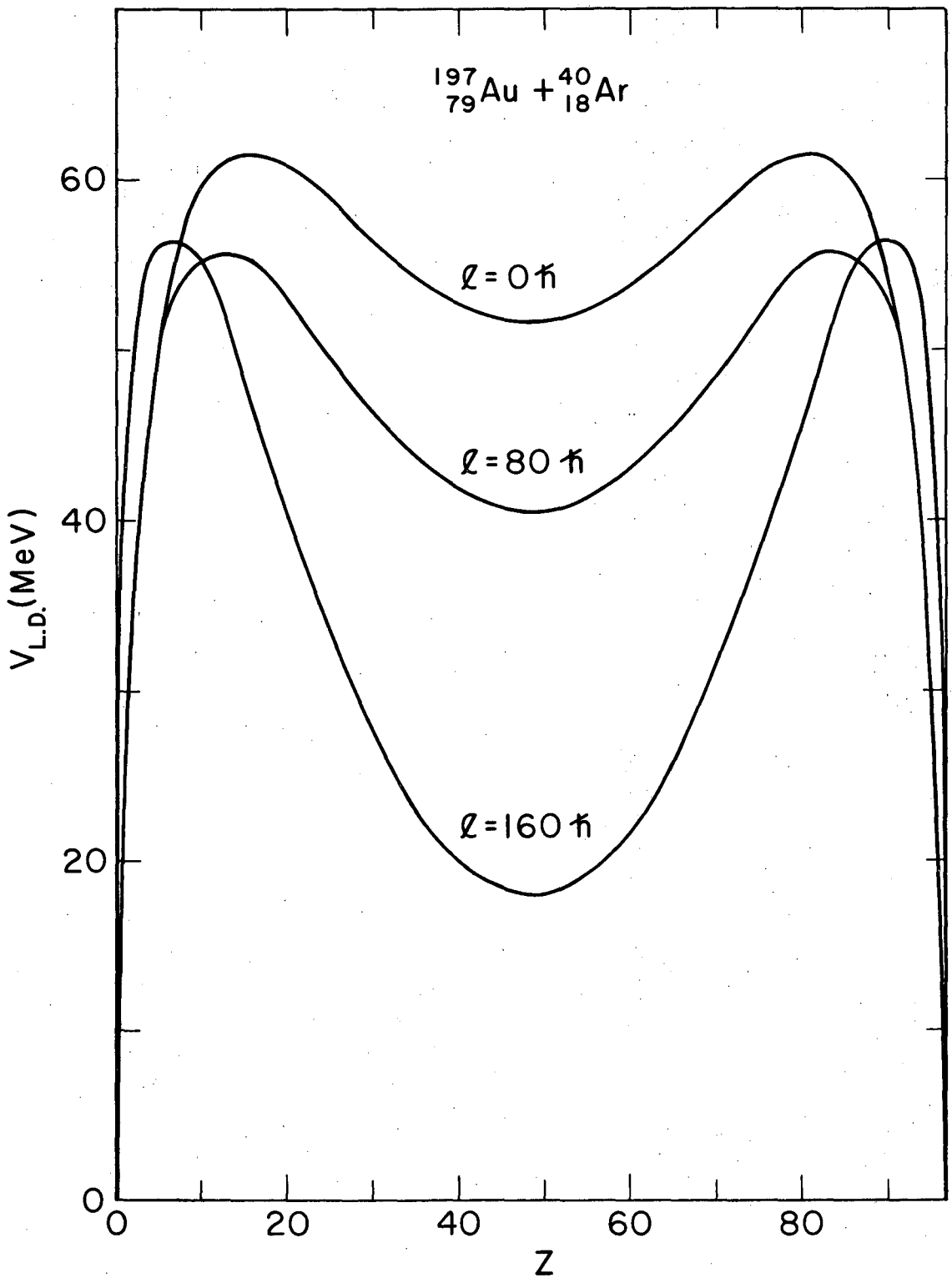

Fig. 5

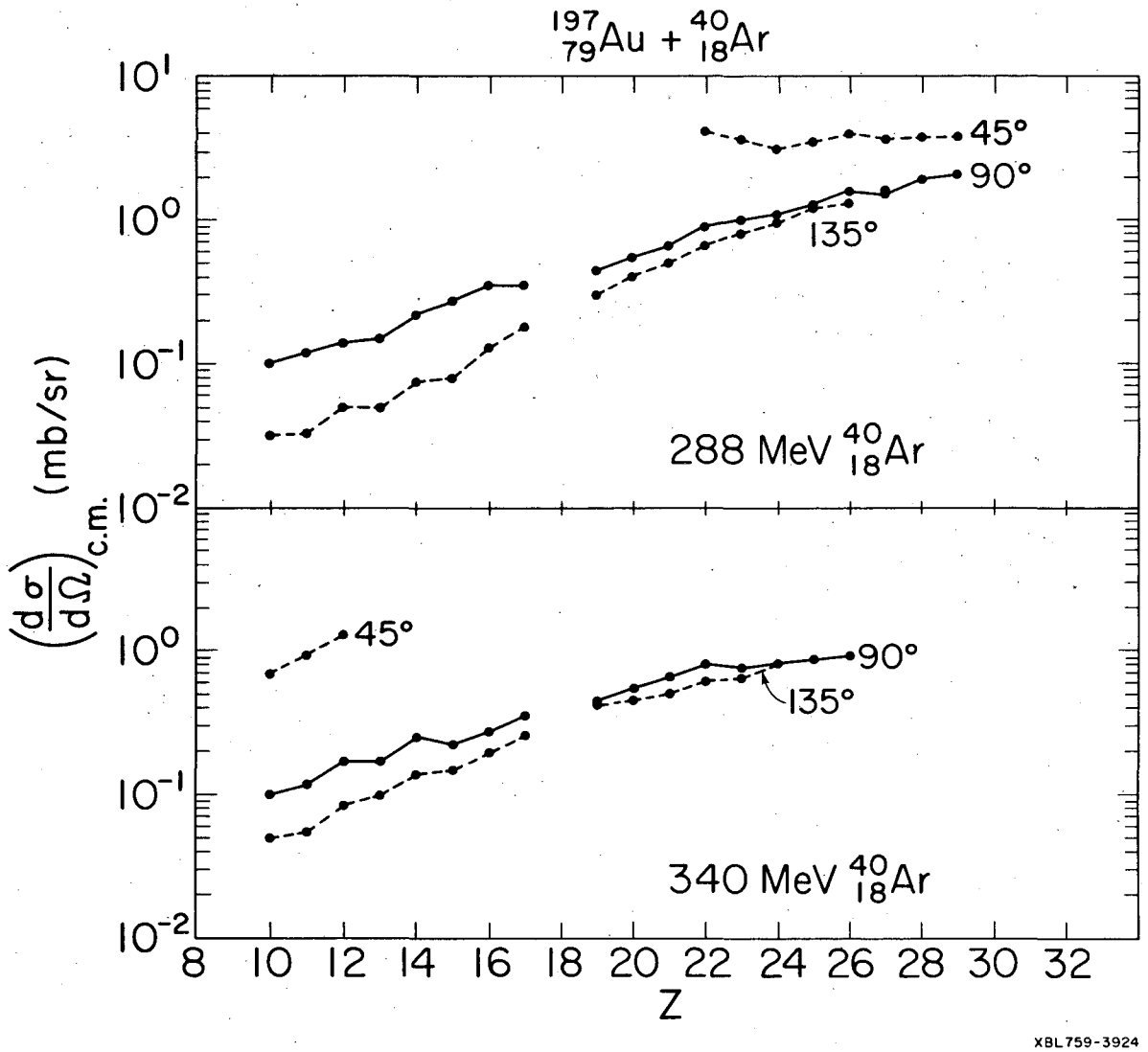
$^{197}_{79}Au + ^{40}_{18}Ar$
10^1
10^0
10^{-1}
10^{-2}
45°
90°
135°
288 MeV $^{40}_{18}Ar$
340 MeV $^{40}_{18}Ar$
$\left(\frac{d\sigma}{d\Omega}\right)_{c.m.}$ (mb/sr)
8 10 12 14 16 18 20 22 24 26 28 30 32
Z
XBL759-3924

Fig. 6

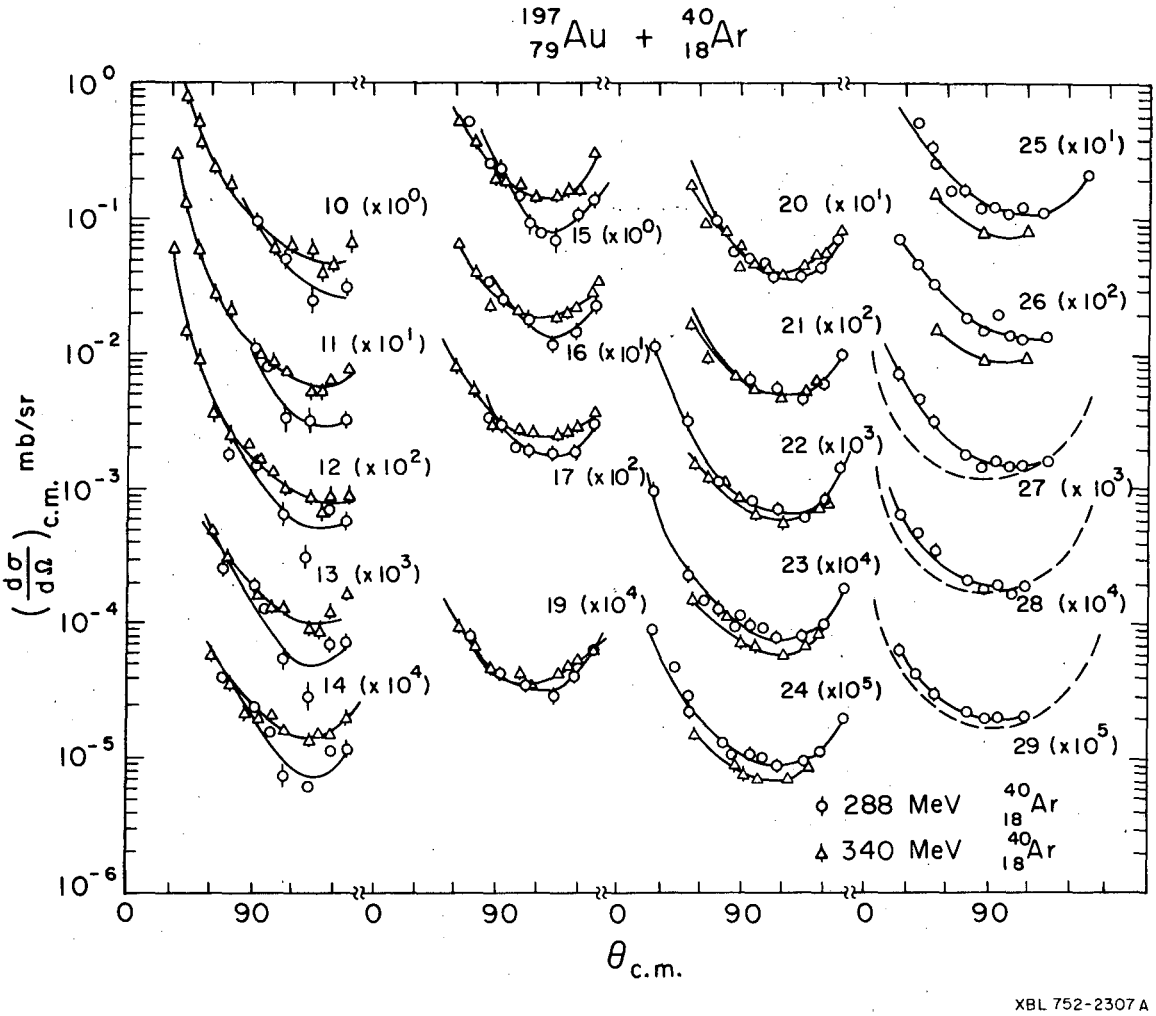

Fig. 7

TECHNICAL INFORMATION DIVISION
LAWRENCE BERKELEY LABORATORY
UNIVERSITY OF CALIFORNIA
BERKELEY, CALIFORNIA 94720